

# Numerical analysis for design of bioinspired ceramic modular armors for ballistic protections

VF González-Albuixech<sup>1</sup>, M Rodríguez-Millán<sup>2</sup> , T Ito<sup>3</sup>,  
JA Loya<sup>3</sup> and MH Miguélez<sup>2</sup>

International Journal of Damage  
Mechanics

2019, Vol. 28(6) 815–837

© The Author(s) 2018

Article reuse guidelines:

[sagepub.com/journals-permissions](http://sagepub.com/journals-permissions)

DOI: 10.1177/1056789518795203

[journals.sagepub.com/home/ijd](http://journals.sagepub.com/home/ijd)



## Abstract

The exigent requirements for personal protections in terms of energy absorption and ergonomics have led to increasing interest in bioinspired protections. This work focuses on the numerical analysis of ballistic behavior of different bioinspired geometries under impact loadings. Ceramic armors based on ganoid fish scales (the type exhibited by gars, bichirs and reedfishes), placoid fish scales (characterizing sharks and rays) and armadillo natural protection have been considered. Different impact conditions are studied, including perpendicular and oblique impacts to surface protection, different yaw angle, and multiple impacts. Main conclusion is related to the improved efficiency of modular armors against multiple shots exhibiting more localized damage and crack arrest properties. Moreover, its potential ergonomic is a promising characteristic justifying a deeper study.

## Keywords

Numerical analysis, bioinspired armors, impact loadings, damage, ceramic protections

## Introduction

The increased terrorism activity has translated war scenarios involving ballistic threats to European cities. Penetration capability of hard-cored armor-piercing ammunition, leads to increase requirements of personal protections for law enforcement agents combining both elevated resistance against penetration and ergonomics.

The optimum armor solutions against ballistic threats range from polymer composites for the less penetrative projectiles to ceramic-faced polymer composites for higher velocity and harder types (Woodhead Publishing Limited, 2012). Ceramics exhibit low density, high hardness, high rigidity,

---

<sup>1</sup>Centro de Investigación en Ingeniería Mecánica, Universitat Politècnica de València, Valencia, Spain

<sup>2</sup>Department of Mechanical Engineering, University Carlos III of Madrid, Madrid, Spain

<sup>3</sup>Department of Continuum Mechanics and Structural Analysis, University Carlos III of Madrid, Madrid, Spain

### Corresponding author:

VF González-Albuixech, Universitat Politecnica de Valencia, camino de Vera s/N, Valencia 46022, Spain.

Email: [vigonal@upv.es](mailto:vigonal@upv.es)

and compressive strength, causing projectile fragmentation and erosion dispersing the kinetic energy (Woodhead Publishing Limited, 2012). Alumina is one of the most used ceramic types in the defense sector, due to its competitive cost-to-efficiency rate (Ponižnik et al., 2017).

In modular armors, the ceramic tiles are joined to a backing plate based on metal or composite (commonly based on aramid fibers) (Pandya et al., 2015). Thus, the increased armor performance is because of the combination of the erosive effect of the ceramic and the composite and energy absorption capability of the backing plate.

Although ballistic behavior of protections has been widely studied in the literature (Pandya et al., 2015; Rostamiyan and Ferasat, 2017; Shaktivesh et al., 2015), ergonomics is also an important issue to be accounted specially when the protection is used during long periods. On the other side, the protective performance of the armor under multiple shots is a crucial requirement. Only few works have been focused on this important aspect of the protection (Deka et al., 2009; Grujicic and Coutries, 2012; Russell, 2014). Deka et al. (2009) carried out experimental tests and numerical simulations in order to investigate the response of laminated composites subjected to high velocity and multi-site impacts. They concluded that the sequential impact resulted in a 23.0% and 14.2% increase in delamination damage over simultaneous impact for two and three projectile impacts, respectively. Russell (2014) investigated multi-impact of projectiles on thin 304 stainless steel plates in order to assess the degradation of ballistic performance. Grujicic and Coutries (2012) studied numerically the multi-hit ballistic-protection performance of a transparent glass/polycarbonate laminate armor, demonstrating the influence of prior bullet shots in reducing armors ballistic-protection performance.

Bioinspired protections based on modular architecture can provide impact resistance to single and multiple shots and mobility due to their flexible configuration. Currently, it is possible to find modular ceramic structures with the aim of resisting multiple impacts (e.g. Chintapalli et al., 2014; Peel, 2015). Chintapalli et al. (2014) analyzed a hexagonal one-layer armor using static analysis and inferring conclusions for impact situations, but not dynamic impact simulations/tests are performed or considered. They considered material properties for a borosilicate glass, but not enough information about the exact composition. Peel (2015) focused on the dragon skin armor using experimental tests. The ceramic module was introduced in pockets of the bulletproof vest in the form of dragon scales, but not material properties are provided for performing simulations. Therefore, due to the sensibility of the material and damage parameters with composition, these lack of properties difficult the possible results comparison between them and other works.

Animal protections are based on multifunctional dermal armors combining protective role with mobility and commodity (Yang et al., 2013). Flexible dermal armor is able to distribute the locally applied load (for instance, by teeth) to a larger region, decreasing stress concentration and damage to the underlying tissue. Therefore, flexible armor based on rigid pieces presents a compromise between protection and mobility. The animals exhibiting natural armors are between others, armadillos or pangolin (mammals), alligators, crocodiles, lizards, turtles (reptiles) and different fishes. Several authors have observed the good performance of these natural armor under impact (Flores-Johnson et al., 2014; Grunenfelder et al., 2014). Fish scales have also been studied showing interesting protective performance (Chintapalli et al., 2014; Liu et al., 2016). Due to the complex geometries involved in the natural armors some studies have been focused on developing designing methodologies for computer simulations (see e.g. Duro-Royoa et al., 2015). All the studies show promising performance, however, also drawbacks on controlling the proper geometry and weight are revealed. Therefore, more effort is necessary prior to implementation of these type of bioinspired protections in current armor design.

Experimental work is extremely costly due to the expensive ceramic components and the difficulty in developing tooling for manufacture prototyping. It is worth noting the importance of geometrical configuration of the bioinspired armor based on the small pieces assembly. Numerical modeling based on finite element method (FEM) is a powerful tool commonly used in armor development helping in the first stages of designing. This paper focuses on the numerical analysis of different configurations of bioinspired ceramic armor being a first stage for a further design. Three-dimensional (3D) finite element models have been developed in order to investigate the response of bioinspired ceramic armor systems against normal, oblique and yaw angle impact of penetrating projectiles. The armor's performance has been compared in terms of depth of penetration (DOP) and damage distribution using the finite element code ABAQUS/Explicit. The considered configurations in the present work are ganoid fish scales (that can be found mainly in gars, bichirs and reedfishes); placoid scales (found in sharks and rays, elasmobranchs), and armadillo protection (dermal bone plates covered by scales called scutes). These configurations are selected due to the promising behavior of these architectures and the lack of studies comparing their performance as can be found for fish scales considered in Chintapalli et al. (2014) and Liu et al. (2016) or for the dermal configuration approximated by the use of composites (Flores-Johnson et al., 2014; Grunenfelder et al., 2014).

Main goal of the present work is the numerical analysis of the response of the outer ceramic layer based on bioinspired armors for ballistic protections. Different ceramic structures (geometry, size, and overlapping) and impact situations (orthogonal, oblique, yaw angle and multi-impact) are studied. All configurations are simulated with a metallic back plate and their performance were compared to that exhibited by a monolithic ceramic plate.

The paper is structured in this introduction, followed by the section 'Description of bioinspired armor configuration' presenting the description of the armor architecture and the ammunition considered in the analysis. Section 'Numerical modelling' describes the numerical models and the validation of the mechanical behavior of the ceramic components. The results are included in section 'Results and discussion' and final conclusions are stated in section 'Conclusions'.

## **Description of bioinspired armor configuration**

The bioinspired armor configurations considered are presented in this section: two kinds of fish scales (with different elemental module geometry and assembly strategy) based on the armadillo natural protection. The selected configurations are approximated using simplified modules, designed accounting for manufacture feasibility. The module dimensions are adjusted to keep approximately the ratio between the different dimensions, and an average thickness of 10 mm, that is the thickness of the monolithic ceramic armor configuration used as a reference for model validation.

### ***Ganoid configuration***

The first modular model is based on ganoid fish scales exhibited by gars, bichirs and reedfishes. They are diamond-shaped scales (see Figure 1), with a multilayer structure: ganoine, dentine, isopedine and a bone basal plate (with total thickness about 400  $\mu\text{m}$ ), being the ganoine the hardest layer (62 GPa) (Bruet et al., 2008). Each module shows two different parts: a diamond-shaped part forming the external barrier and a lower part intended for assembly several modules. Figure 1 shows its dimensions and highlight contact surfaces and the pattern for creating the bioinspired modular armor.

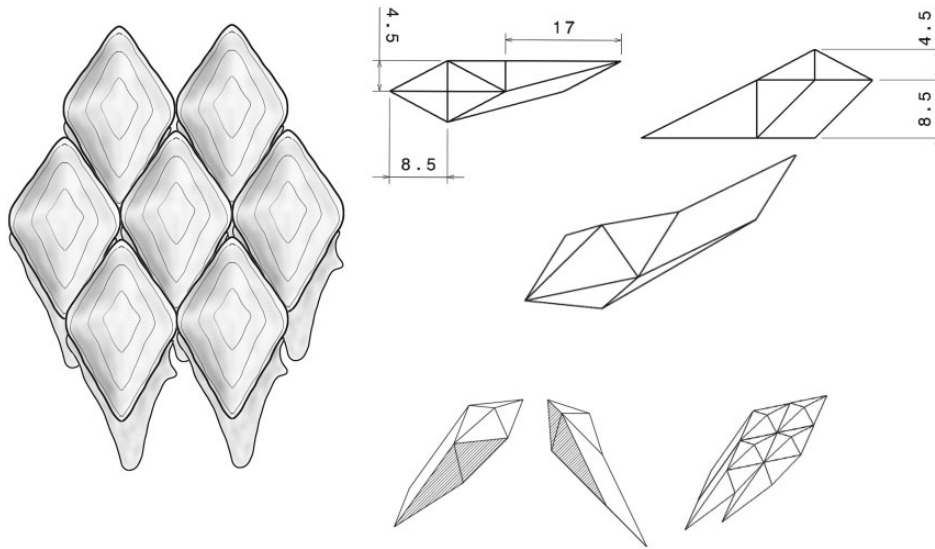


**Figure 1.** Scheme of the ganoid configuration, and assembly pattern of the ganoids inspired modules. Dimensions in mm.

### *Placoid configuration*

The second modular model considered in this work is based on placoid scales, found in sharks and rays (elasmobranchs). These scales are used as protection against predators and, in some sharks, also have a hydrodynamic function. Similar to the human teeth, they have an inner core made of connective tissues, blood vessels and nerves. They are covered by a dentine layer and a hard outer layer of vitrodentine. The exposed surface is covered with a hard enamel layer (Porter et al., 2017), which Young's modulus, measured using indentations, ranges from approximately 3 to 6 GPa and 70 to 120 GPa, respectively (Bajaj and Arola, 2009). The scales are supported by spines attached to a rectangular basal plate that rests on the skin (Figure 2). The module geometry is simplified for computational costs and manufacturability. The modules present an indentation and a beak for limiting any vertical movement. Module shape and their assembly are displayed in Figure 2.

### *Armadillo configuration*

The armadillo armor consists of dermal bone plates covered by scutes acting as a defense against predators (Figure 3). The armadillo has a unique protective body armor, called the osteoderm, which confers to its shell-like skin distinctive mechanical properties (Chen et al., 2011). The tough and highly mineralized tiles have a Young's modulus of 425 MPa, a tensile strength of approximately 20 MPa and toughness of around 1 MJ/m<sup>3</sup>. The modules are similar to bands assembled together. Dimensions of a module, and the assembly scheme, can be observed in Figure 3.

## **Numerical modelling**

In this section, the modeling strategies for the simulation of the projectile and the modular armor behavior are presented. The mechanical properties of the different components of the model are

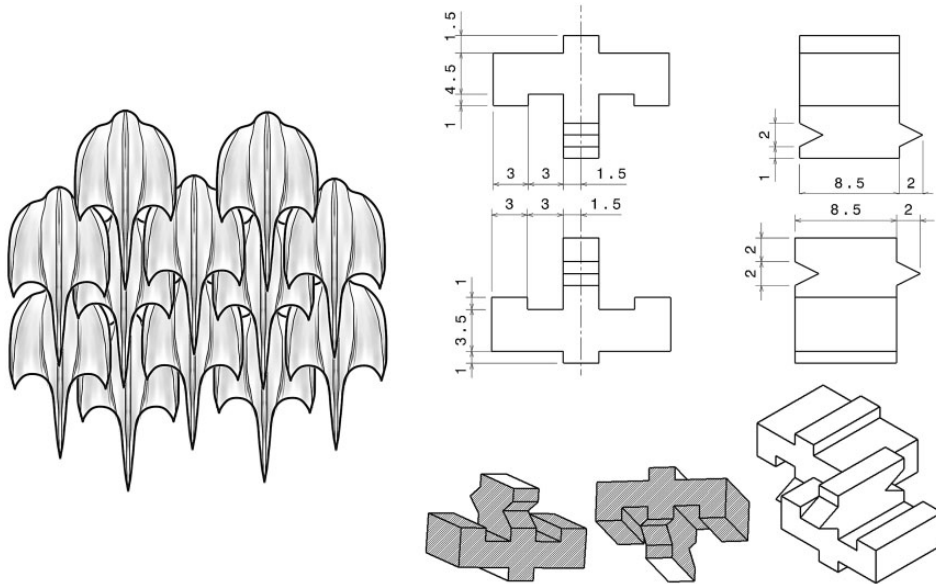


**Figure 2.** Scheme of the placoid configuration. Elemental module and assembly reproducing placoid scale. Dimensions in mm.

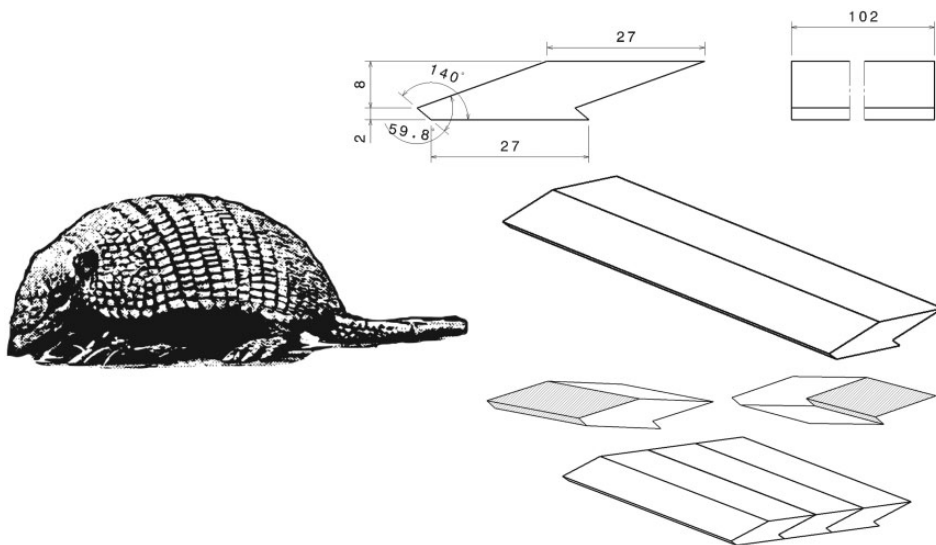


**Figure 3.** Scheme of the armadillo configuration. Elemental module reproducing armadillo module. Dimensions in mm.

calibrated and validated comparing to experimental results available in the literature (Reaugh et al., 1999). Once the numerical models faithfully predict the experimental results, bioinspired armors configurations are compared to each other. Contact between target components is modeled using non-penetration algorithms available in the FE code.

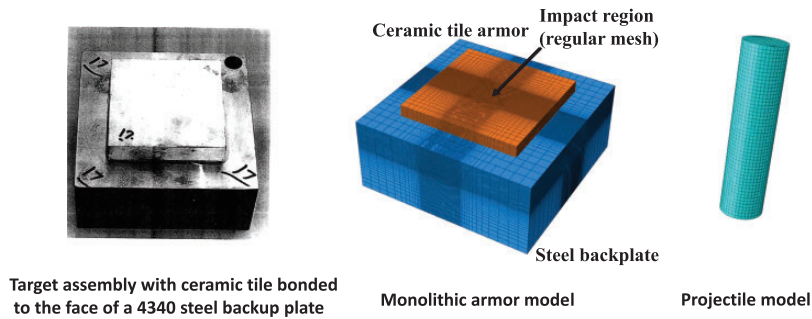


**Figure 4.** Validation case for monolithic armor and projectile. Experimental target set up (Reaugh et al., 1999), and numeric model.

### Projectile

The projectile is defined as a cylinder with aspect ratio length/diameter ( $L = 25.4$  mm,  $D = 6.35$  mm) equal to 4, which is an intermediate value between long rods and short projectiles being representative of a wide range of different ammo. The rod material is defined as tungsten sinter-alloy W2, according to Reaugh et al. (1999). The projectile model, shown in Figure 4, is meshed using C3D8R (hexahedrons) with element size equal to 0.5 mm.

### Numerical model for calibration of ceramic behavior

The mechanical behavior of the ceramic is calibrated according to ballistic tests on a monolithic plate of ceramic (alumina 96) joined to a back plate made of steel 4340, described in Serjouei (2015). Dimensions of the target are  $102 \times 102 \times t$  mm<sup>3</sup> for the ceramic tile with variable thickness ( $t$  ranges from 10.5 mm to 30.2 mm), and  $152 \times 152 \times 64$  mm<sup>3</sup> for the steel plate. The experimental set up and the model meshes are shown in Figure 4. The experimental and numerical results are compared in terms of DOP in the steel block.

The ceramic tile is meshed with hexahedrons (elements denoted C3D8R in ABAQUS/Explicit), with a size defined in two regions. The mesh is refined at the zone around the impact area defined by a square of  $30 \times 30$  mm<sup>2</sup> with element size of 0.5 mm while, out of this region the element size is increased, in normal direction is also 0.5 mm.

The steel plate is meshed using hexahedrons. The element size is defined in the same way in two regions, a region corresponding to the impact zone, given by a  $35 \times 35 \times 24$  mm<sup>3</sup>. The ceramic tile is located over the steel plate, imposing non-penetrating contact between adjacent surfaces.

### Bioinspired armor: Modeling ceramic modular component and metallic back plate

The models reproducing bioinspired protection combine a metallic back plate and the ceramic elements substituting the monolithic plate modeled as a reference case. In all cases, ceramic part is located over the steel plate, and no penetrating contact conditions are imposed between contacting surfaces. The reference thickness and average thickness of both the bioinspired modules and the reference monolithic plate are stated equal to 10.0 mm.

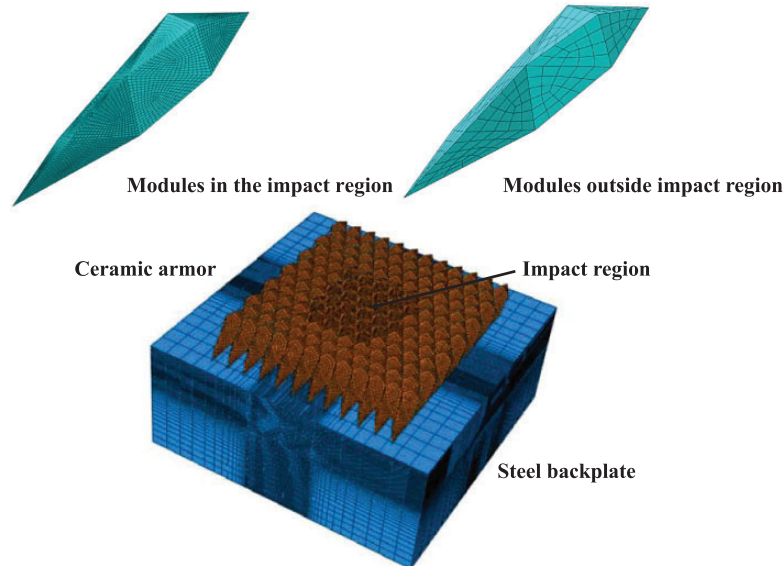


**Figure 5.** Detail of module meshing and assembled plate for ganoid armor.

**Ceramic monolithic armor.** The model of the ceramic monolithic armor used for model calibration is also used as a reference for comparison to the bioinspired configuration (details have been previously described, see Figure 4).

**Ganoid modular armor.** Modules are meshed independently using hexahedron elements. Element size in the impact area ( $30 \times 30 \text{ mm}^2$ ) is 0.5 mm while outside of the impact zone coarser elements is used. Finally, the modules are assembled onto the back layer forming a plate based on discrete pieces. Details of the module mesh and assembled plate are illustrated in Figure 5.

**Placoid modular armor.** Modules are meshed in a similar way than that described for the ganoid armor using structured hexahedrons as regular as possible. The average size of the elements at the impact region is 0.5 mm, while coarser elements are defined out of this region. The modules are assembled on the back layer forming a plate as it is detailed in Figure 6.

**Armadillo modular armor.** Modules are meshed using hexahedrons with element size 0.5 mm at the impact region while the element size increases out of the impact area. Bands are assembled on the back layer as it is shown in Figure 7.

### Materials modelling

**Metallic components.** The thermoviscoplastic mechanical behavior of the metallic alloys in the back plate and also in the projectile is modeled using the Johnson–Cook (JC) equation (Johnson and Cook, n.d.). The JC model available in the commercial code used in this work (ABAQUS/Explicit) is

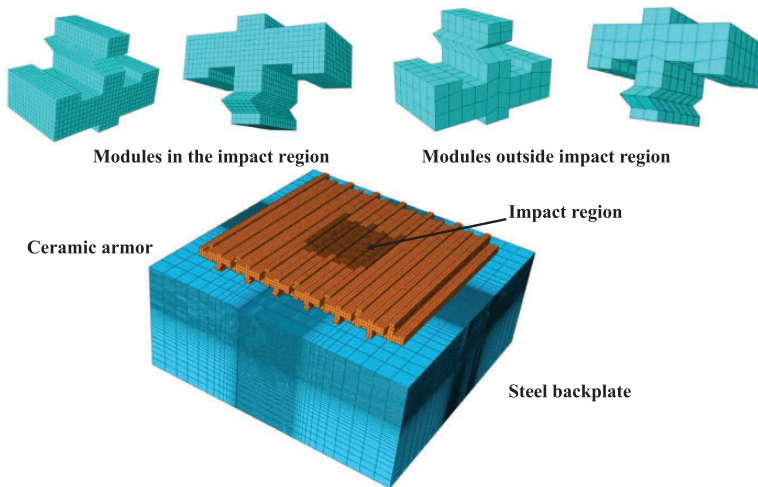


**Figure 6.** Detail of module meshing and assembled plate for the placoid armor.

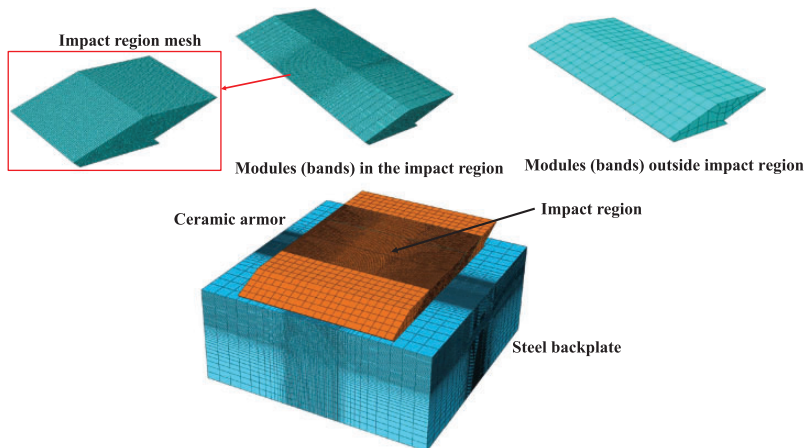


**Figure 7.** Detail of band and assembly meshes for the armadillo inspired armor.

defined in equations (1) and (2). The first term defines strain hardening ( $\bar{\varepsilon}^p$ ), the second strain rate sensitivity ( $\dot{\varepsilon}^p$ ) and the third one is related to the thermal softening ( $\Theta$ ):

$$\bar{\sigma}(\bar{\varepsilon}^p, \dot{\varepsilon}^p, T) = [A + B(\bar{\varepsilon}^p)^n] \left[ 1 + C \ln \left( \frac{\dot{\varepsilon}^p}{\dot{\varepsilon}_0} \right) \right] [1 - \Theta^m] \quad (1)$$

where  $A$ ,  $B$ ,  $C$ ,  $n$  and  $m$  are material constants,  $\dot{\varepsilon}_0$  is a user-defined reference strain rate,  $\Theta$  depends on the current temperature  $T$ , being  $T_m$  the melting temperature, and  $T_0$  a reference temperature:

$$\Theta = \frac{T - T_0}{T_m - T_0} \quad (2)$$



Material failure is introduced through the criterion of JC, which is based on damage accumulation,  $D$ , as shown in equation (3).

$$D = \sum_i \frac{\Delta \bar{\varepsilon}_i^p}{\varepsilon_f} \quad (3)$$

where  $D$  is the damage in the element,  $\Delta \bar{\varepsilon}_i^p$  is the increment of accumulated plastic strain on loading step  $i$  summed over the loading steps, and  $\varepsilon_f$  is the plastic strain to failure defined in equation (4).

$$\bar{\varepsilon}_f(\eta, \dot{\bar{\varepsilon}}^p, \Theta) = [D_1 + D_2 \exp(-D_3 \eta)] \left[ 1 + D_4 \ln \left( \frac{\dot{\bar{\varepsilon}}^p}{\dot{\varepsilon}_0} \right) \right] [1 + D_5 \Theta] \quad (4)$$

where  $D_i$  are failure parameters and  $\eta$  is the stress triaxiality.  $D$  is used as criterion for element deletion ( $D = 1.0$ ), when  $\bar{\varepsilon}_f$  reaches the critical value given in equation (4).

The parameters of the constitutive equation and failure models are obtained from Serjouei (2015) for the cases of steel (back plate) and tungsten (projectile) (see Tables 1 and 2).

**Ceramic components.** The Johnson–Holmquist-2 (JH-2) constitutive model (D. Systemes, 2012; Johnson and Holmquist, 1993), is used to reproduce the ceramic mechanical behavior under large

**Table 1.** Mechanical properties of steel 4340.

$\rho_0$ (kg/m <sup>3</sup> )	7830	$\varepsilon_0$ (s <sup>-1</sup> )	1
$E$ (GPa)	159	$D_1$	0.05
$\nu$	0.32	$D_2$	3.44
$A$	792	$D_3$	2.12
$B$	51	$D_4$	0.0002
$n$	0.26	$D_5$	0.61
$m$	1.03	$C$	0.014
$T_m$ (K)	1793	$T_{trans}$ (K)	300

**Table 2.** Mechanical properties of projectile tungsten alloy.

$\rho_0$ (kg/m <sup>3</sup> )	18,360	$\varepsilon_0$ (s <sup>-1</sup> )	1
$E$ (GPa)	310	$D_1$	0.0
$\nu$	-0.03	$D_2$	0.033
$A$	1506	$D_3$	1.5
$B$	177	$D_4$	0.0
$n$	0.12	$D_5$	0.0
$m$	1	$C$	0.016
$T_m$ (K)	1723	$T_{trans}$ (K)	300

strain, high-strain rate, and high pressure conditions. The model consists of three terms describing strength, pressure and damage. Strength is expressed using the normalized von Mises equivalent stress as it is formulated in equation (5).

$$\sigma^* = \sigma_i^* - D(\sigma_i^* - \sigma_f^*) \quad (5)$$

where  $\sigma_i^*$  is the normalized intact equivalent stress,  $\sigma_f^*$  is the normalized fractured equivalent stress and  $D$  is the damage. The normalized stresses are given in the generalized form  $\sigma^* = \sigma/\sigma_{HEL}$ , where  $\sigma$  is the von Mises equivalent stress and  $\sigma_{HEL}$  is the equivalent stress at the Hugoniot Elastic Limit (HEL). The normalized intact and fractured equivalent stresses are formulated in equations (6) and (7), respectively.

$$\sigma_i^* = A(P^* + T^*)^N(1 + C \ln \dot{\epsilon}^*) \quad (6)$$

$$\sigma_f^* = M(P^*)^M(1 + C \ln \dot{\epsilon}^*) \quad (7)$$

where  $A$ ,  $B$ ,  $C$ ,  $M$ ,  $N$  are material parameters. The normalized pressure is defined as  $P^* = P/P_{HEL}$ , with  $P$  being the actual pressure and  $P_{HEL}$  the pressure at the HEL. The maximum tensile hydrostatic pressure is  $T^* = T/P_{HEL}$  where  $T$  is the maximum tensile pressure that the material can withstand. The normalized strain rate is defined as  $\dot{\epsilon}^* = \dot{\epsilon}/\dot{\epsilon}_0$  where  $\dot{\epsilon}$  is the current strain rate and  $\dot{\epsilon}_0 = 1.0$  is a reference strain rate. The pressure density relationship is introduced in equation (8).

$$P = K_1\mu + K_2\mu^2 + K_3\mu^3 \quad \text{if } \mu \geq 0 \quad (8)$$

$$P = K_1\mu \quad \text{if } \mu \leq 0 \quad (9)$$

where  $\mu = \rho/\rho_0 - 1$ . The model includes the effect of dilatation or bulking that appears with the brittle material failure, as an additional pressure increment, equation (10)

$$P = K_1\mu + K_2\mu^2 + K_3\mu^3 + \Delta P \quad (10)$$

$\Delta P$  is determined by energy considerations in equation (11)

$$\Delta P_{t+\Delta t} = -K_1\mu_{t+\Delta t} + \sqrt{(K_1\mu_{t+\Delta t} + \Delta P_t) + 2\beta K_1 \Delta U} \quad (11)$$

where  $\beta$  is the fraction of elastic energy loss converted to potential hydrostatic energy, equal to 1 in the present case.

The damage  $D$  accumulates with plastic strain according to equation (12)

$$D = \frac{\Delta \bar{\epsilon}_i^{pl}}{\bar{\epsilon}_f^{pl}} \quad (12)$$

$\Delta \bar{\epsilon}_i^{pl}$  is the equivalent plastic strain increment on loading step  $i$  summed over the loading steps, and  $\bar{\epsilon}_f^{pl}$  is the equivalent plastic strain to fracture under constant pressure defined by equation (13)

$$\bar{\epsilon}_f^{pl} = D_1(P^* + T^*)^{D_2} \quad (13)$$

**Table 3.** Alumina material parameters for JH-2 model.

$\rho$	3850 kg/m <sup>3</sup>	$G$	152 GPa
$A$	0.88	$n$	0.64
$B$	0.45	$m$	0.6
$C$	0.007	$T$	0.462 GPa
$P_{HEL}$	4 GPa	$\beta$	1
$D_1$	0.0125	$D_2$	0.7
$K_1$	231 GPa	$K_2$	−160 GPa
$K_3$	774 GPa		

JH-2: Johnson–Holmquist-2.

$D_1$  and  $D_2$  are material parameters.

The selected material for this analysis is Alumina 96% ( $Al_2O_3$ ), which parameters, obtained from Klasztorny and Swierczewski (2012), Morka and Nowak (2012) and Serjouei (2015), are presented in Table 3. The material parameters are verified using the experimental data in Serjouei (2015) and Reaugh et al. (1999).

## Results and discussion

The performance of the armor configurations is analyzed using numerical modeling. Several impact conditions corresponding to normal, and oblique impacts (with or without yaw angle), and multiple impacts are simulated. The obtained numerical results are compared with experimental data (Reaugh et al., 1999), or with the reference configuration in terms of the DOP and damaged volume in the steel plate.

### Model validation

The ceramic material behavior is validated with experimental data of ceramic tiles subjected to ballistic impact, reported in Reaugh et al. (1999). The calibration/validation is based on the comparison between DOP in the steel block obtained from the numerical simulation, illustrated in Figure 8, and the experimental DOP reported in Reaugh et al. (1999). Table 4 summarizes experimental and numerical predictions of DOP for the monolithic ceramic tile. Especially close to the thickness equal to 10 mm, assumed as a reference thickness and average thickness for the bioinspired modules, results show good agreement.

### Numerical results for bioinspired configuration

Two parameters are considered in order to analyze the armor performance. For each armor, the dimensionless depth of penetration ( $DOP_{dim}$ ) (equation (14)), is defined as the ratio between the depth obtained ( $DOP_{armor}$ ) and the reference depth obtained for the monolithic ceramic plate ( $DOP_{monolithic}$ ). The second parameter of interest is the dimensionless damaged volume ratio,  $DV_{dim}$ , defined as the ratio between the damaged volume in the backing material for each modular configuration and the obtained for the monolithic

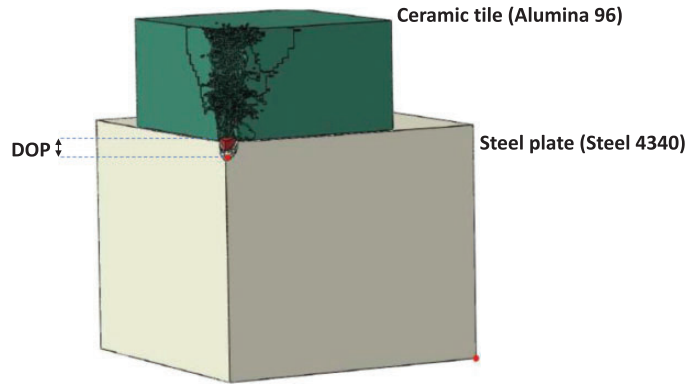


**Figure 8.** Scheme of the DOP estimation for the numerical simulations.  
DOP: depth of penetration.

**Table 4.** DOP comparison between numerical model and experimental results for ceramic model validation.

Tile thickness (mm)	Initial velocity (m/s)	Exp. DOP (mm)	Num. DOP (mm)
10.5	1350	14.5	15.0
20.6	1360	8.7	11.0
30.2	1360	4.0	6.2

DOP: depth of penetration.

case, considered as the reference value. The  $DV_{dim}$  is computed from the elements with  $D = 1.0$  (equation (3)).

$$DOP_{dim} = \frac{DOP_{armor}}{DOP_{monolithic}} \quad (14)$$

$$DV_{dim} = \frac{DV_{armor}}{DV_{monolithic}} \quad (15)$$

**Orthogonal impact.** The first set of simulations corresponds to normal impact, i.e. the projectile impact direction is orthogonal to the armor ceramic plane with initial impact velocity set to  $v_0 = 1350$  m/s. The following situations are considered: a bullet revolutionary axis orthogonal to the impact plane  $\alpha = 0^\circ$ , and a bullet which axis defines a yaw angle of  $\alpha = 30^\circ$  from the orthogonal direction to the plane of the target. Real bullet commonly experiences yaw deviations, thus the second case analyzed in this section is more realistic reproducing service conditions. As it was explained previously, the average thickness for each ceramic configuration is 10 mm. The scheme of the simulated configurations is presented in Figure 9.

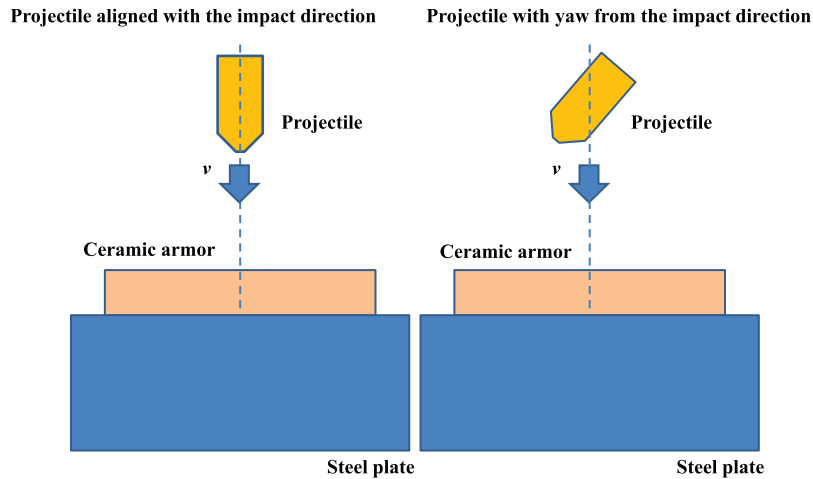


**Figure 9.** Scheme of simulated normal impacts.

**Table 5.**  $DOP_{dim}$  ratio for orthogonal impacts and different yaw angle.

Configuration	Placoid	Ganoid	Armadillo
$\alpha = 0^\circ$	1.28	1.09	1.06
$\alpha = 30^\circ$	1.13	1.12	0.95

$DOP_{dim}$ : dimensionless depth of penetration.

**Table 6.** Steel dimensionless damaged volume ratio for orthogonal impact and different yaw angle.

Configuration	Placoid	Ganoid	Armadillo
$\alpha = 0^\circ$	1.60	2.05	1.85
$\alpha = 30^\circ$	1.31	1.10	1.58

The  $DOP_{dim}$  of each configuration (equation (14)) is presented in Table 5. It can be observed that the  $DOP_{dim}$  is higher for the armor with smaller modules, especially in the case of a direct impact. In case of a bullet with a certain yaw angle, the modular armor behaves quite similar to the monolithic armor. The smaller modules offer less individual protection.

The dimensionless damaged volume ratio (equation (15)) is presented in Table 6. The damaged patterns for each configuration are illustrated in Figures 10 and 11. Modular armors produced lower effect on projectile erosion, however, they give better performance for wider impact region. Meanwhile, the monolithic plate can be regarded as destroyed after impact, damaged ceramic is highly localized on the armor with small modules and does not propagate to the regions not directly affected by the impact. This behavior is important for the case of multiple shots, and the possibility of repairing a reduced area instead of replacing the entire ceramic plate.

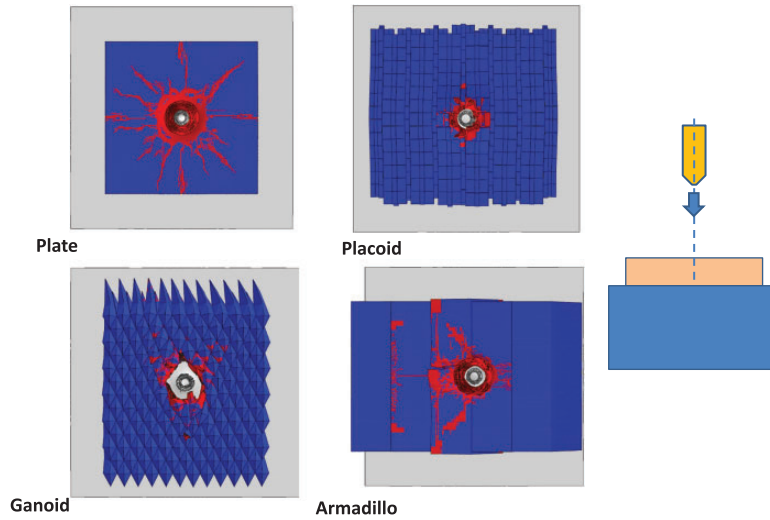


**Figure 10.** Damage distribution on ceramic for the orthogonal impact and bullet aligned with the impact trajectory. Damaged in red, undamaged in blue.

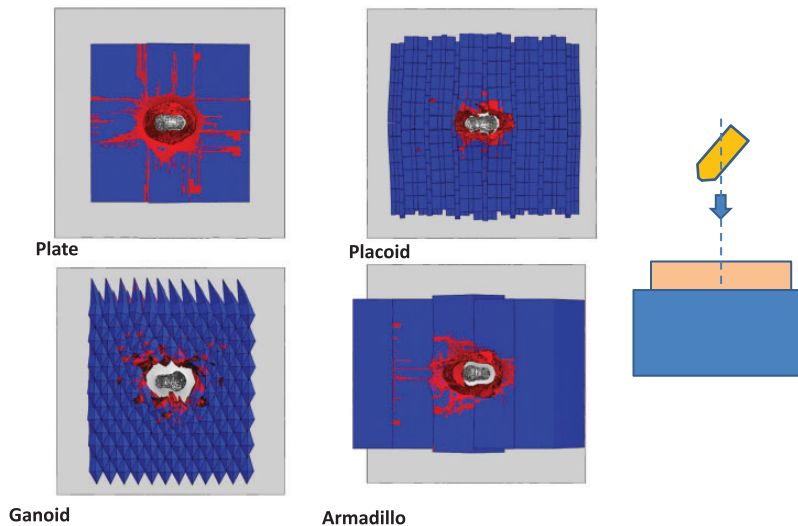


**Figure 11.** Damage distribution on ceramic for the orthogonal impact, and bullet with yaw from the impact trajectory,  $\alpha = 30^\circ$ . Damaged elements in red, undamaged in blue.

**Oblique impact.** The second set of simulations corresponds to oblique impact situations, i.e. the projectile impact direction is oblique with respect to the armor ceramic plane, the deviation from this plane is  $30^\circ$ . The initial impact velocity is set to  $v_0 = 1350$  m/s as it was explained previously. Cases with bullet axis aligned with the impact velocity direction and yaw angle equal to  $\alpha = 30^\circ$  are also considered. The oblique impact is better approximation to real service conditions, including

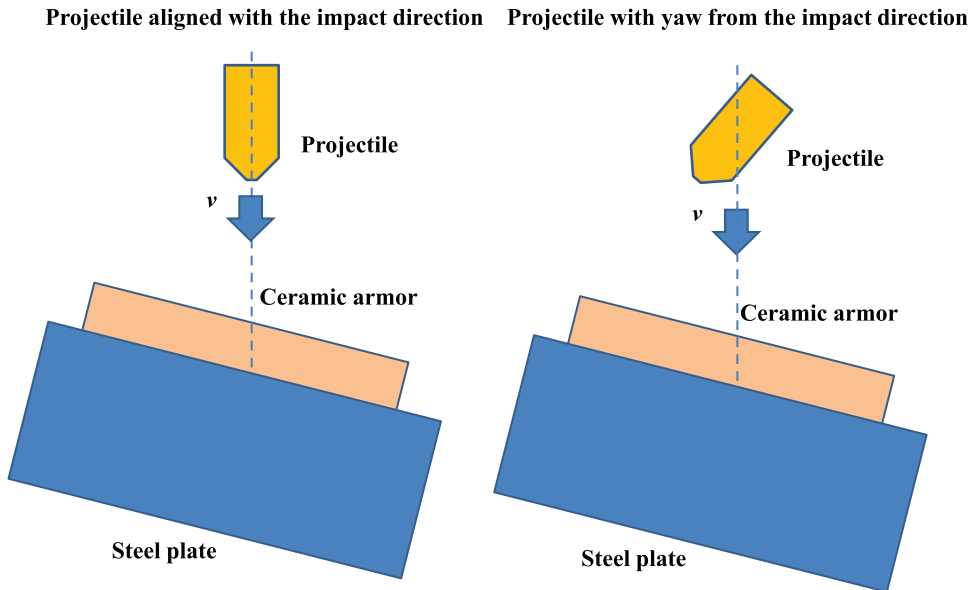


**Figure 12.** Scheme of simulated oblique impacts.

**Table 7.**  $DOP_{dim}$  for oblique impacts and different yaw angle.

Configuration	Placoid	Ganoid	Armadillo
$\alpha = 0^\circ$	1.16	1.26	1.08
$\alpha = 30^\circ$	1.05	1.12	1.01

$DOP_{dim}$ : dimensionless depth of penetration.

fragments from explosion, as it is commented previously. Scheme of the simulated configurations is presented in Figure 12.

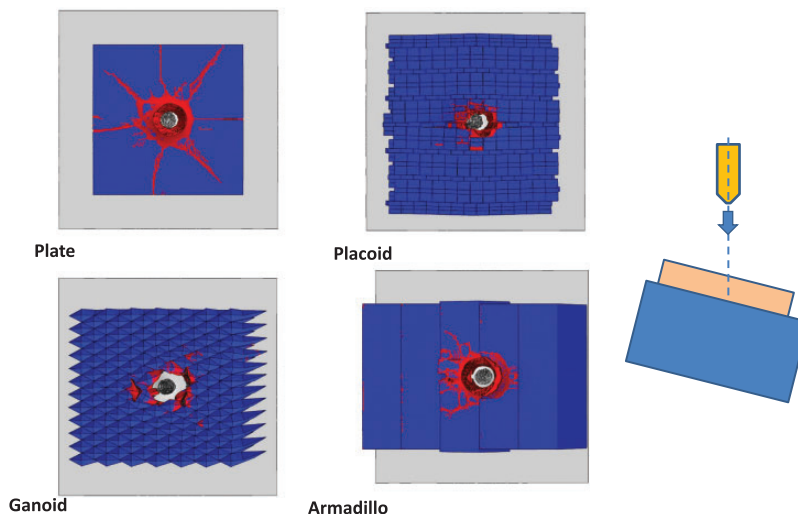
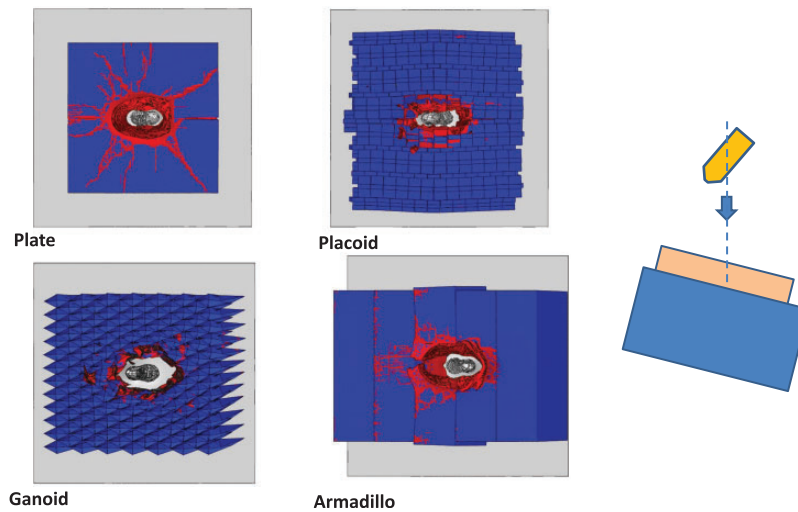
$DOP_{dim}$  (equation (14)) results are presented in Table 7. The dimensionless DOP is slightly higher for smaller modules armor, but since the impact is oblique, the entanglement between different modules also plays an important role, explaining the better comparative performance for the placoid configuration. The armadillo armor configuration shows almost the same performance in terms of  $DOP_{dim}$  as the monolithic plate.

The results for steel dimensionless damaged volume ratio,  $DV_{dim}$  (equation (15)), are presented in Table 8. The ceramic damaged area is illustrated in Figures 13 and 14.

Steel normalized damage extension ratio is always higher in the modular armors in comparison to the monolithic plate. This is related to localization of damage in the modular configuration. However, this is an advantage for prevention of the loss of efficiency of the armor out of the impact region. As it is reported in the former case, the monolithic plate can be considered destroyed after the impact. It is highlighted that the protective role of the modular armors is slightly worse (1–8%) but close to the monolithic plate behavior making them suitable for light weapons ammunition.

**Table 8.** Steel dimensionless damaged volume ratio for oblique impacts and different yaw angle.

Configuration	Placoid	Ganoid	Armadillo
$\alpha = 0^\circ$	1.48	2.21	1.60
$\alpha = 30^\circ$	1.72	1.16	1.94

**Figure 13.** Damage distribution on ceramic for the oblique impact and bullet aligned with the impact trajectory. Damaged elements in red, undamaged in blue.**Figure 14.** Damage distribution on ceramic for the oblique impact, and bullet with yaw from the impact trajectory,  $\alpha = 30^\circ$ . Damaged elements in red, undamaged in blue.



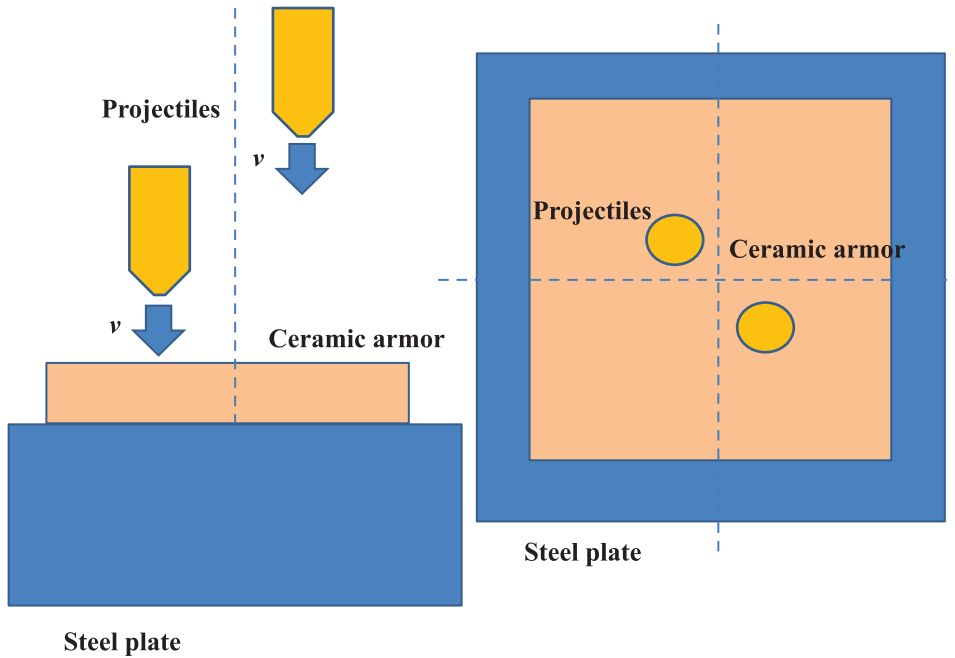


**Figure 15.** Scheme of simulated double impacts.

**Table 9.**  $DOP_{dim}$  ratio for double impacts.

Configuration	Placoid	Ganoid	Armadillo
First impact	1.12	1.12	0.96
Second impact	1.03	1.01	0.88

$DOP_{dim}$ : dimensionless depth of penetration.

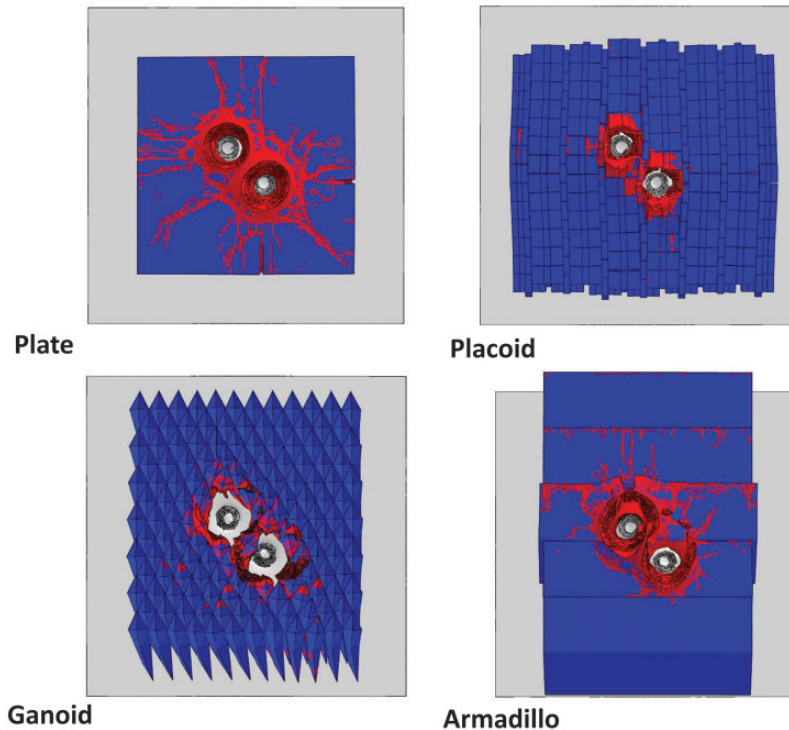
### Multiple impacts

Last simulations set considers the multi-shot case consisting of two bullets impacting subsequently the same armor with the same velocity. Multi-hits are reported to affect the performance of the armors, and occur under real fire situation (automatic weapons, or fragments in explosion, for instance). The trajectory of both projectiles is assumed to be orthogonal to the upper plane of the armor. The initial impact velocity is set to  $v_0 = 1350$  m/s. The distance between both bullets impact trajectory axis is 17.5 mm. A scheme of the simulated configurations is presented in Figure 15.

The  $DOP_{dim}$  values for each projectile are presented in Table 9, being slightly worse for the first impact, as expected; however, it is almost the same or better for the second impact. The change on protection ratio in comparison to the first impact, can be related to the remaining protective role of the modules, as the damaged for each impact is more concentrated, and therefore the modules not directly affected still retain some protective properties in comparison to the monolithic plate armor.

**Table 10.** Steel dimensionless damaged volume ratio for double impacts.

Configuration	Placoid	Ganoid	Armadillo
Double impact	1.71	2.57	1.83

**Figure 16.** Damage distribution on ceramic for the oblique impact and bullet aligned with the impact trajectory. Damaged elements in red, undamaged in blue.

Steel dimensionless damaged volume ratio is presented in Table 10. Ceramic damaged area is observed in Figure 16. The steel normalized damage extension ratio in the armors is higher than in the monolithic case. It is remarkable that the damaged ceramic region is still lower than for the monolithic plate, and therefore, if a third impact would occur, the modular armor would exhibit some protection. Therefore, modules maintain its protective role on multi-hit situations in comparison to monolithic armors, even accepting that its overall protection is slightly lower for just one impact. These results are significant for long-term operations.

### *Armadillo armor module analysis*

According to aforementioned results, the protection based on armadillo armor shows a good performance in ballistic terms. For this reason, a deeper study is carried out in this section. The effects

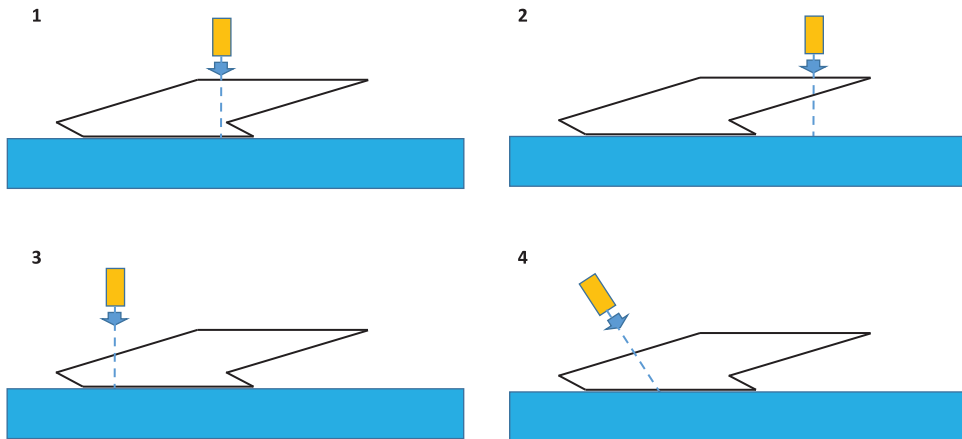


**Figure 17.** Geometrical scheme of simulated impacts considering only one module for the armadillo armor.

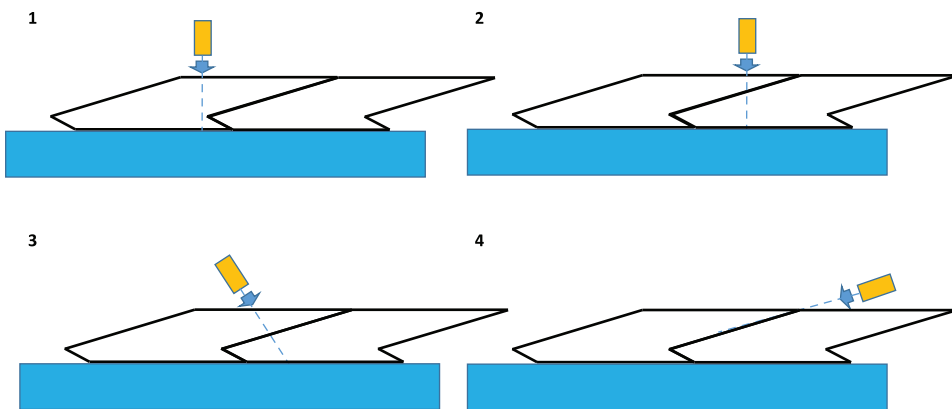


**Figure 18.** Geometrical scheme of simulated impacts considering only two module for the armadillo armor.

**Table II.**  $DOP_{dim}$  ratio for module analysis.

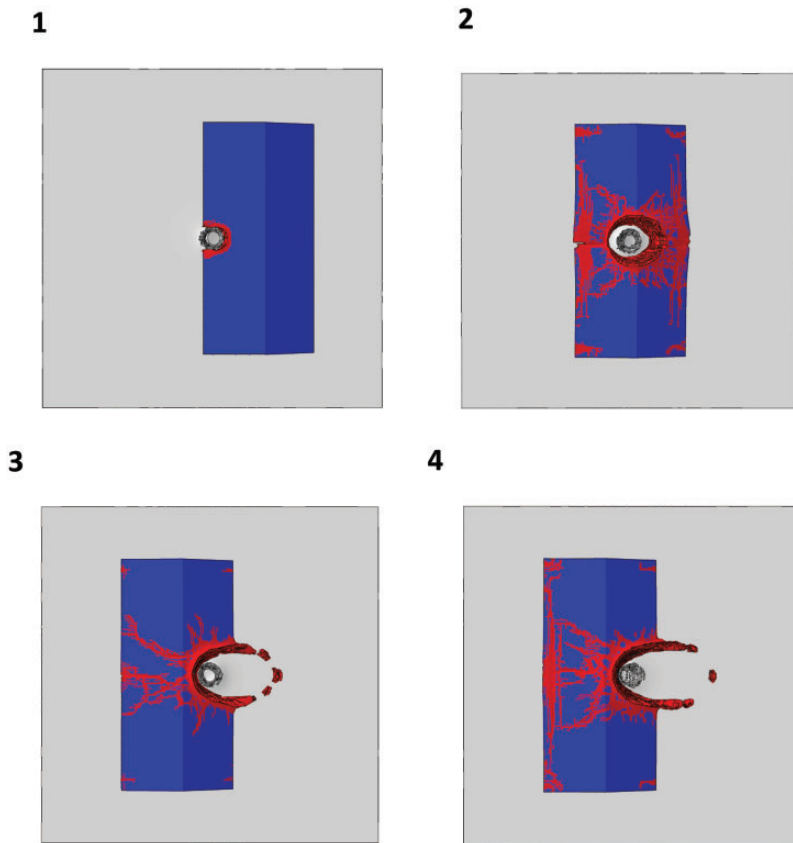
Configuration	1	2	3	4
One module	1.04	1.44	1.13	1.26
Two modules	1.01	1.04	1.03	0.87

$DOP_{dim}$ : dimensionless depth of penetration.

of the impact on different parts of a module and the case for several modules influence are investigated. The scheme of the analyzed impact directions and relative positions for one and two modules configurations are schemed in Figures 17 and 18, respectively. The initial impact velocity is set to  $v = 1350$  m/s.

**Table 12.** Steel dimensionless damaged volume ratio for module analysis.

Configuration	1	2	3	4
One module	1.80	2.00	2.25	1.87
Two modules	2.15	2.20	1.52	1.67

**Figure 19.** Damage pattern on ceramic for the oblique impact and bullet aligned with the impact trajectory (upper view). Damaged elements in red, undamaged in blue.

The  $DOP_{dim}$  for each configuration is presented in Table 11. The  $DOP_{dim}$  shows that the ballistic performance of modules can be comparable to the obtained with a same thickness monolithic plate.

Steel dimensionless damaged volume ratio is presented in Table 12. Ceramic damaged area is observed in Figures 19 and 20. In every considered case, the obtained damage is smaller than in the case where the monolithic plate is considered. It is highlighted that in the configuration 4 for two modules, the projectile bounces after the impact. It is an effect due to the difference on erosion by the bottom module and the top plate as the projectile advances thorough the union, and shows that, in some cases, the presence of seams might be even advantageous.

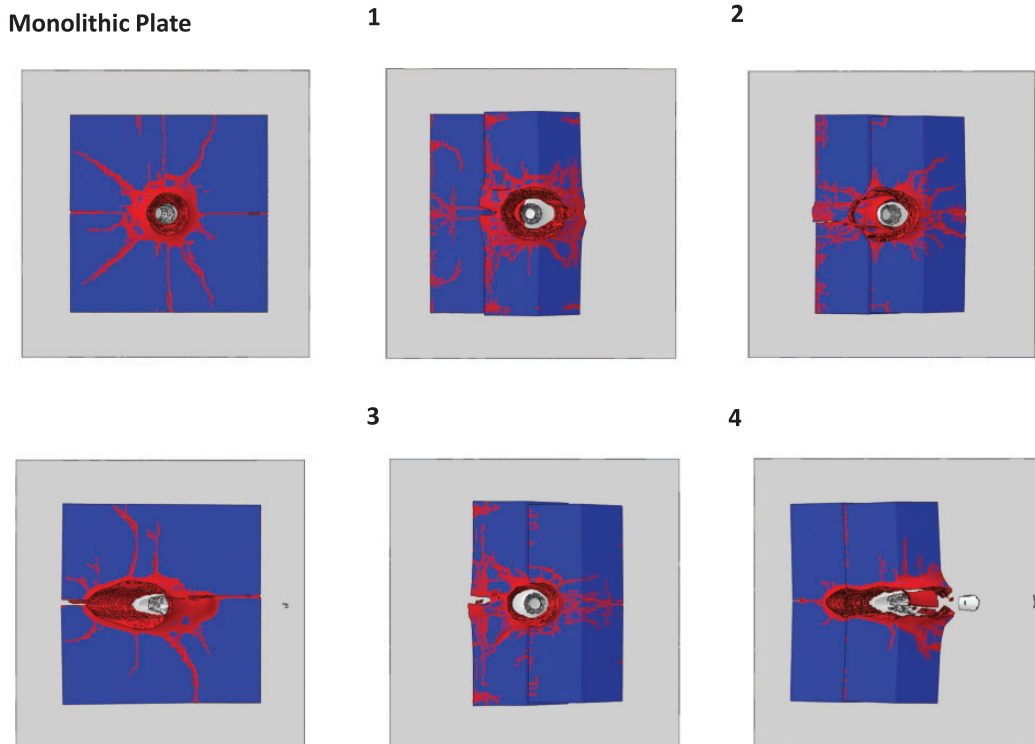


**Figure 20.** Damage pattern on ceramic for the oblique impact and bullet aligned with the impact trajectory (upper view). Damaged elements in red, undamaged in blue.

## Conclusions

In this paper, bioinspired modular armors for ballistic protections have been analyzed using numerical modelling based on FEM. The considered armors cover several geometries, module size, and module overlapping. Different impact situations (orthogonal, oblique and yaw deviations) have been studied in order to analyze the armor performance on realistic service conditions.

The protection performance evaluated in the back plate in terms of  $DOP_{dim}$  and damaged volume,  $DV_{dim}$ , showed that the modular armors performance was slightly lower than that exhibited by the monolithic plate. However, the damage on the armor was confined close to the impact zone and thus, the modular configuration maintained its protective performance in case of multiple impacts. Hence, in combat situations, modular armors would provide advantages respect to the monolithic ones, since those retained protective performance for subsequent shots.

Moreover, the possibility of a partial replacement for reparation after shooting is also an interesting advantage. Bioinspired modular protections also owe the advantage for ergonomic design, being critical in long-term usage of the protection.

Armor based on armadillo structure presented higher performances in terms of the analyzed parameters in this work, being an alternative to monolithic ceramic tile. In fact, armadillo armor improved by 4% in terms of penetration depth to the monolithic structure for a first impact and up to 12% for the second impact. In other hand, the architectures based on placoid and ganoid presented worse performance for the first impact, showing similar results to the monolithic structure in

the second one. However, no direct performance comparison has been feasible with results provided by other authors due to differences in the material and armor geometries analyzed.


### Declaration of conflicting interests

The author(s) declared no potential conflicts of interest with respect to the research, authorship, and/or publication of this article.

### Funding

The author(s) disclosed receipt of the following financial support for the research, authorship, and/or publication of this article: This work has been carried out within the framework of the research program Juan de la Cierva Incorporación 2015, and research projects DPI2017-88166-R, and RTC-2015-3887-8 of FEDER program financed by the Ministerio de Economía, Industria y Competitividad of Spain. The support of the Generalitat Valenciana, Programme PROMETEO 2016/007 is also acknowledged.

### ORCID iD

M Rodríguez-Millán  <http://orcid.org/0000-0002-9081-8425>.

### References

- Bajaj D and Arola DD (2009) On the R-curve behavior of human tooth enamel. *Biomaterials* 30: 4037–4046.
- Bruet BJB, Song J, Boyce MC, et al. (2008) Materials design principles of ancient fish armour. *Nature Materials* 7: 748–756.
- Chen IH, Kiang JH, Correa V, et al. (2011) Armadillo armor: Mechanical testing and micro-structural evaluation. *Journal of the Mechanical Behavior of Biomedical Materials* 4: 713–722.
- Chintapalli RK, Mirkhalaf M, Dastjerdi AK, et al. (2014) Fabrication, testing and modeling of a new flexible armor inspired from natural fish scales and osteoderms. *Bioinspiration and Biomimetics* 9(3): 036005.
- D. Systemes (2012) *Abaqus v6.12 Documentation*. Providence, RI: ABAQUS Inc.; 6.12.
- Deka L, Bartus S and Vaidya U (2009) Multi-site impact response of s2-glass/epoxy composite laminates. *Composites Science and Technology* 69(6): 725–735.
- Duro-Royoa J, Zolotovskiy K, Mogas-Soldevila L, et al. (2015) MetaMesh: A hierarchical computational model for design and fabrication of biomimetic armored surfaces. *Computer-Aided Design* 60: 14–27.
- Flores-Johnson E, Shen L, Guimatsia I, et al. (2014) Numerical investigation of the impact behaviour of bioinspired nacre-like aluminium composite plates. *Composites Science and Technology* 96: 13–22.
- Grujicic DPM and Coutries N (2012) A computational investigation of the multi-hit ballistic-protection performance of laminated transparent-armor systems. *Journal of Materials Engineering and Performance* 21(6): 1–12.
- Grunenfelder L, Suksangpanya N, Salinas C, et al. (2014) Bio-inspired impact-resistant composites. *Acta Biomaterialia* 10(9): 3997–4008.
- Johnson G and Cook W (1983) A constitutive model and data for metals subjected to large strains high strain rates and high temperatures. In: *Proceedings of the seventh international symposium on ballistics*, The Hague, Netherlands, 19–21 April 1983, pp. 541–547. Hubei Province, China: SCIRP.
- Johnson G and Holmquist T (1993) An improved computational constitutive model for brittle materials. In: Schmidt SC, Shaner J, Samara GA and Ross M (eds) *High pressure science and technology – 1993. Institute of physics conference proceedings*, vol. 309, Colorado Springs, Colorado, USA, 28 June–2 July 1993, pp.981–994.
- Klasztorny M and Swierczewski M (2012) Numerical modelling and validation of 12.7 mm FSP impact into ALFC shield – ARMOX 500T steel plate system. *Journal of KONES Powertrain and Transport* 19(4): 291–299.
- Liu P, Zhu D, Yao Y, et al. (2016) Numerical simulation of ballistic impact behavior of bio-inspired scale-like protection system. *Materials and Design* 99: 201–210.

- Morka A and Nowak J (2012) Numerical analyses of ceramic/metal ballistic panels. *Journal of KONES Powertrain and Transport* 19(4): 465–492.
- Pandya KS, Kumar CVS, Nair NS, et al. (2015) Analytical and experimental studies on ballistic impact behavior of 2D woven fabric composites. *International Journal of Damage Mechanics* 24(4): 471–511.
- Peel KS (2015) *Dragon Skin How it Changed Body Armor Testing in the United States Army Naval Postgraduate*. Monterey, CA: Naval Postgraduate School.
- Ponižnik Z, Nowak Z and Basista M (2017) Numerical modeling of deformation and fracture of reinforcing fibers in ceramic–metal composites. *International Journal of Damage Mechanics* 26(5): 711–734.
- Porter MM, Ravikumar N, Barthelat F, et al. (2017) 3D-printing and mechanics of bio-inspired articulated and multi-material structures. *Journal of the Mechanical Behavior of Biomedical Materials* 73: 11426.
- Reaugh J, Holt A, Cunningham BW, et al. (1999) Impact studies of five ceramic materials and pyrex. *International Journal of Impact Engineering* 23: 771–782.
- Rostamiyan Y and Ferasat A (2017) High-speed impact and mechanical strength of ZrO<sub>2</sub>/polycarbonate nanocomposite. *International Journal of Damage Mechanics* 26(7): 989–1002.
- Russell B (2014) Multi-hit ballistic damage characterisation of 304 stainless steel plates with finite elements. *Materials and Design* 58: 252–264.
- Serjouei A (2015) Empirical ballistic limit velocity model for bi-layer ceramic–metal armor. *International Journal of Protective Structures* 6(3): 509–527.
- Shaktivesh, Nair NS and Naik NK (2015) Ballistic impact behavior of 2D plain weave fabric targets with multiple layers: Analytical formulation. *International Journal of Damage Mechanics* 24(1): 116–150.
- Woodhead Publishing Limited (2012) *Advances in Military Textiles and Personal Equipment*. Cambridge, UK: Woodhead Publishing.
- Yang W, Chen IH, Gludovatz B, et al. (2013) Natural flexible dermal armor. *Advanced Materials* 25(1): 31–48.